

# Lawrence Berkeley National Laboratory

LBL Publications

Title

Nanoscale Confinement of Photo-Injected Electrons at Hybrid Interfaces

Permalink

<https://escholarship.org/uc/item/8m05j8tw>

Journal

The Journal of Physical Chemistry Letters, 12(49)

ISSN

1948-7185

Authors

Neppl, Stefan

Mahl, Johannes

Roth, Friedrich

et al.

Publication Date

2021-12-16

DOI

10.1021/acs.jpcelett.1c02648

Peer reviewed

# Nanoscale Confinement of Photo-Injected Electrons at Hybrid Interfaces

*Stefan Neppel<sup>1,‡,†</sup>, Johannes Mahl<sup>1,2,†</sup>, Friedrich Roth<sup>3</sup>, Giuseppe Mercurio<sup>2,§</sup>, Guosong Zeng<sup>1,4</sup>,  
Francesca M. Toma<sup>1,4</sup>, Nils Huse<sup>2</sup>, Peter Feulner<sup>5</sup>, and Oliver Gessner<sup>1,\*</sup>*

<sup>1</sup>Chemical Sciences Division, Lawrence Berkeley National Laboratory, Berkeley, CA 94720, USA

<sup>2</sup>Physics Department, Universität Hamburg and Center for Free-Electron Laser Science, 22761 Hamburg, Germany

<sup>3</sup>Institute of Experimental Physics, TU Bergakademie Freiberg, 09599 Freiberg, Germany

<sup>4</sup>Liquid Sunlight Alliance, Lawrence Berkeley National Laboratory, Berkeley, CA 94720, USA

<sup>5</sup>Physics Department, Technische Universität München, 85748 Garching, Germany

<sup>†</sup>these authors contributed equally to this work

<sup>‡</sup>current affiliation: Paul Scherrer Institut, 5232 Villigen, Switzerland

<sup>§</sup>current affiliation: European XFEL, 22869 Schenefeld, Germany

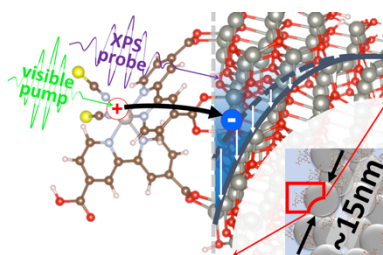
---

\*email: ogessner@lbl.gov

## ABSTRACT

A prerequisite for advancing hybrid solar light harvesting systems is a comprehensive understanding of the spatio-temporal dynamics of photo-induced interfacial charge separation. Here, we demonstrate access to this transient charge redistribution for a model hybrid system of nanoporous zinc oxide (ZnO) and ruthenium bipyridyl chromophores. The site-selective probing of the molecular electron donor and semiconductor acceptor by time-resolved X-ray photoemission provides direct insight into the depth distribution of the photo-injected electrons and their interaction with the local band structure on a nanometer length-scale. Our results show that these electrons remain localized within less than 6 nm from the interface, due to enhanced downward band-bending by the photo-injected charge carriers. This spatial confinement suggests that light-induced charge generation and transport in nanoscale ZnO photocatalytic devices proceeds predominantly within the defect-rich surface region, which may lead to enhanced surface recombination and explain their lower performance compared to titanium dioxide (TiO<sub>2</sub>)-based systems.

## TOC GRAPHICS



**KEYWORDS** Interfacial charge transfer; Time-resolved X-ray Photoelectron Spectroscopy; Hybrid light harvesting systems; Band bending;

Nanostructured metal oxide semiconductor materials coupled to light-harvesting adsorbates are key components in sunlight-to-power and sunlight-to-fuel conversion schemes. Examples include photochemical cells for solar water-splitting and hybrid photovoltaics based on heterojunctions between molecular, quantum-dot, or nanoplasmonic sensitizers and transition metal oxide semiconductor electrodes.<sup>1-6</sup> These systems combine superior solar light absorption in the adsorbates with high photocatalytic activity of the substrates and the heterogeneous design enables spatial separation of oxidation and reduction half-reactions. Yet, observed efficiencies consistently lack, often substantially, behind theoretical limits. Understanding the photo-induced electron transfer and relaxation dynamics between sensitizers and semiconductor acceptors is crucial for advancing photocatalytic efficiency. This challenge encompasses the full photocatalytic reaction cycle: ultrafast charge injection, carrier transport and interfacial charge relaxation, as well as trapping at defect centers within the nanoporous semiconductor network. The complex interplay of these microscopic processes, and the vast range of relevant time- and length-scales, render it difficult to unambiguously identify reaction bottlenecks that limit the overall device performance.<sup>7,8</sup>

The timescale of the initial charge separation at the interface plays a decisive role, and has been extensively studied, mainly with all-optical techniques that monitor the transient electronic state of the sensitizer and the appearance of free electrons inside the semiconductor.<sup>9-16</sup> However, very little is known about the underlying transient interfacial charge density redistribution, associated band structure modifications, and their spatio-temporal evolution within the first few nanometers below the surface. The band structure at the interface can be different from the bulk due to local space-charge imbalances that affect all energy levels near the

surface. This potential energy landscape can either enhance interfacial charge separation of injected electrons (upward band bending) or favor their confinement and localization near the surface (downward band bending).<sup>17</sup> Since the near-surface region represents a significant volume fraction of nanostructured systems, it is the main gateway between localized photoexcited states on the sensitizers and delocalized charge distributions in the semiconductor that drive chemical reactions.

The hybrid interface between nanostructured ZnO and N3 (cis-bis(isothiocyanato)bis(2,2'-bipyridyl-4,4'-dicarboxylato)-ruthenium(II)) dye molecules offers a model system for understanding the complex interaction of photo-induced charge injection, separation, and transfer. ZnO-based nanomaterials are important components in photocatalytic devices,<sup>18</sup> and N3 is one of the most widely studied molecular sensitizers for hybrid light harvesting systems.<sup>19,20</sup> Thus, a more detailed understanding of the photo-induced electronic dynamics in N3/ZnO heterosystems provides technologically pertinent benchmarks for a variety of photoelectrochemical applications.

Here, we directly monitor the photo-induced electron dynamics and ensuing transient modulations of near-surface potential gradients in the interfacial region of this prototypical hybrid light harvesting system with picosecond time-resolved X-ray photoelectron spectroscopy (trXPS). Our model system consists of an N3 dye monolayer chemisorbed on a sintered film of ZnO nanoparticles with an average particle diameter of ~15 nm (see supplemental information (SI), section A). Element-specific trXPS probes the transient interfacial electronic structure after optical excitation site-selectively from the molecular electron donor (C1s/Ru3d) and the

semiconductor acceptor (Zn3d) with picosecond temporal resolution and nanometer spatial sensitivity.

The measurements provide detailed information on the spatial distributions of both electrons and holes across the interface during the photo-induced charge transfer and recombination on timescales ranging from tens of picoseconds up to several microseconds. Nanoscale confinement of photo-injected electrons within <6 nm from the semiconductor surface is deduced from transient changes in the surface potentials, which are revealed by lineshape modulations and spectral shifts of the Zn3d photoemission. The C1s/Ru3d response of the molecular donor exhibits an additional transient shift due to the impact of the (electronic) hole located on the photo-oxidized dye. A charged capacitor model is used to describe the charge-separated state at the N3/ZnO interface, from which the average distance of the hole density from the substrate surface is estimated to ~0.3 - 1.2 nm. This range is in agreement with the location of the highest occupied molecular orbital (HOMO), from which the injected electron is removed. Furthermore, strong evidence is provided that electron injection into the ZnO conduction band (CB) proceeds via a two-step process involving an intermediate interfacial charge transfer (ICT) configuration. The existence of such transient ICT states has previously been suggested,<sup>9-12,21-24</sup> but has been in competition with a two-state injection model, where intramolecular relaxation by intersystem crossing precedes electron transfer to the substrate.<sup>25-27</sup>

The results provide comprehensive insight into the spatio-temporal evolution of the photo-induced interfacial charge redistribution. Both the intermediate ICT configurations as well as the confinement of injected electrons in the defect-rich surface region of the nanostructured substrate significantly increase the odds for charge recombination and, thus, contribute to the challenges of

using ZnO as electrode material in solar light harvesting applications. The lifetime of the ICT intermediate as well as the range of electron-dye cation recombination timescales determined here by trXPS are in reasonable to good agreement with values derived in previous time-resolved optical and THz spectroscopy studies.<sup>9,10,14,23</sup>

In the trXPS experiment, the heterojunction is excited by ~10 ps long laser pulses at a wavelength of 532 nm, and the photo-induced dynamics are probed using a monochromatized soft X-ray pulse train from the Advanced Light Source (ALS), see Materials and Methods for details. Figure 1 compares C1s/Ru3d (a) and Zn3d (b) trXPS spectra associated with the N3-dye and the ZnO substrate, respectively. Data (circles) were recorded before (blue) and  $\Delta t = 2$  ns after (red) resonant HOMO-LUMO (lowest unoccupied molecular orbital) excitation of the dye with a 532 nm, 1.1 mJ/cm<sup>2</sup> laser pulse, leading to an estimated 6% excitation fraction (see section G of the SI). Details of the fit procedures (solid lines) and the decomposition of the C1s/Ru3d spectrum<sup>21,28</sup> are described in section B of the SI. For both regions, the excited-state (ES) spectrum is shifted to higher binding energies ( $E_B$ ) compared to the ground state (GS) spectrum. However, the ~180 meV photo-induced shift of the N3-related C1s/Ru3d photoemission lines is significantly larger than the corresponding Zn3d shift of only ~65 meV.

The photoresponses of the two sides of the heterojunction also differ in their lineshape dynamics. The C1s/Ru3d ES spectrum is well described by a rigid shift of the GS spectrum. Figure 1(c) shows the difference between the C1s/Ru3d ES spectrum and the GS spectrum shifted by 180 meV to higher  $E_B$ , indicating good agreement within the signal-to-noise ratio of the experiment. Note that this rigid shift does not exclude smaller differential shifts between C1s and Ru3d as previously found for  $\Delta t \leq 1$  ps.<sup>21</sup> In contrast, a similar approximation for the ES Zn3d

spectrum by a shifted GS spectrum yields a significant residual (black line in Fig. 1(d)), which points toward an additional lineshape change. This effect is captured by including a spectral broadening of the GS spectrum in addition to a shift, as indicated by the corresponding orange

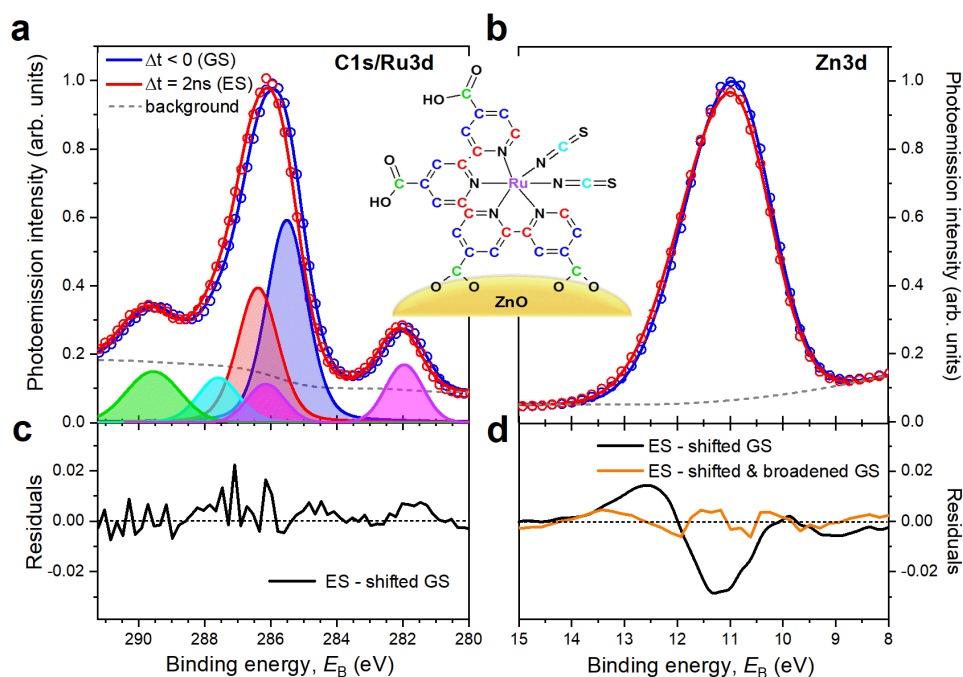


**Figure 1.** Signatures of photo-induced charge transfer in trXPS spectra of N3/ZnO heterojunction. **a** N3-dye C1s/Ru3d and **b** substrate Zn3d trXPS spectra obtained with  $h\nu = 888$  eV and  $h\nu = 614$  eV, respectively. Blue circles are the ground state (GS) spectra, red circles represent the excited state (ES) measured at a pump-probe delay of  $\Delta t = 2$  ns after 532 nm laser excitation. Solid lines correspond to constrained multi-peak Gaussian fits for C1s/Ru3d, and fits to an asymmetric Gaussian for Zn3d. The color-coded schematic of the N3 dye molecular structure in the inset indicates the different contributions to the C1s/Ru3d spectrum. **c** Residual after subtracting the C1s/Ru3d GS spectrum shifted by  $\sim 180$  meV to higher  $E_B$  from the ES spectrum. **d** Minimum residual for the Zn3d photoemission line using the same approach. The distinct bimodal shape indicates significant ES spectral broadening. The orange line is the minimum difference spectrum obtained by including a spectral broadening of  $\sim 65$  meV in addition to a rigid shift of  $\sim 60$  meV.

residual in Fig. 1(d). Figure S3 in section B of the SI illustrates and analyzes the signatures of shift and broadening effects in the Zn3d spectrum in greater detail. We emphasize that no laser-induced changes in the Zn3d position or shape are observed for bare ZnO electrodes under laser excitation conditions identical to those of the dye-sensitized samples (see SI section D). This excludes photo-induced electron-hole pair generation within ZnO, mediated by defect levels within the 3.30 eV bandgap, as an explanation for the observed Zn3d trXPS response.<sup>29-31</sup> Thus, the origin of transient modulations in the Zn3d lineshape shown in Fig. 1 and 2 must be directly connected to heterogeneous charge transfer across the N3/ZnO interface.

Fitting the pump-probe delay dependent C1s/Ru3d and Zn3d photolines with a set of model functions provides the temporal evolution of spectral shifts and peak widths as a function of pump-probe delay (see section B of the SI for details). The results are displayed in Fig. 2(a). Time-dependent shifts of the C1s (red) and Zn3d (blue) peaks are shown along with changes in the full-width-at-half-maximum (FWHM) of the Zn3d peak (green). Symbols represent the peak shifts and widths, solid lines indicate fit results based on a coupled rate equation model of the time-dependent electron populations in the N3 LUMO, at the surface (ICT states), and in the ZnO CB. The model is schematically summarized in Fig. 2(b) (see section H of the SI for details). It describes a sequential pathway, whereby the initial HOMO-LUMO excitation ( $k_1$ ) decays to form an ICT configuration ( $k_2$ ), from which electrons are released into the ZnO CB ( $k_3$ ). Possible electron-dye cation recombination pathways from all these intermediates are taken into account. In particular, back-transfer and recombination of electrons injected into the ZnO CB is described by three independent exponential decays ( $k_{5,a}, k_{5,b}, k_{5,c}$ ). The C1s and Ru3d peaks exhibit identical time-dependent shifts and no broadening within the experimental uncertainty

(see SI section B). Thus, we limit our discussion of the molecular response to the energy shifts of the C1s lines associated with the dye. The inset in Fig. 2(a) shows a magnified view of the region near zero pump-probe delay using normalized amplitudes to highlight differences in dynamic trends.

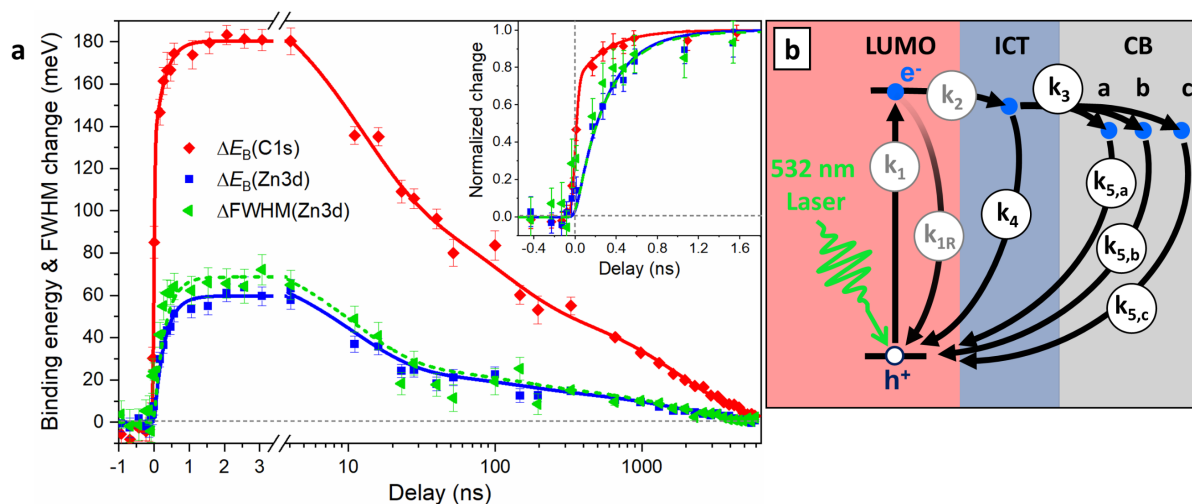


**Figure 2.** **a** Temporal evolution of the trXPS response. C1s (red diamonds) and Zn3d (blue squares) photoelectron energy shifts and Zn3d photoline FWHM change (green triangles) as a function of pump-probe delay (note the transition from a linear to a logarithmic delay axis for  $\Delta t > 3$  ns). Solid lines are the results of fits to a coupled rate equation model schematically illustrated in **b**. Photo-induced HOMO-LUMO excitation ( $k_1$ ) in the dye (red) is followed by the population ( $k_2$ ) of an ICT configuration (blue), and by subsequent electron injection ( $k_3$ ) into the ZnO CB (gray). Recombination of the injected electrons with the dye HOMO holes ( $h^+$ ) involves three rates ( $k_{5,a}$ ,  $k_{5,b}$ ,  $k_{5,c}$ ), corresponding to the three slopes discernible for delays  $> 4$  ns in **a**. The inset in **a** (using normalized amplitudes) highlights the delayed onset of the ZnO responses relative to the N3-dye related response due to the intermediate population of the ICT state. The model is described in more detail in section H of the SI.

A key observation is that the changes in the Zn3d shift and FWHM remain correlated throughout the entire lifetime of the photo-induced effects, from their sub-ns emergence to their final disappearance,  $\sim 6 \mu\text{s}$  after optical excitation. The interpretation of these results requires a more detailed understanding of the composition of the Zn3d spectrum and how it is affected by the photo-induced dynamics. Generally, XPS spectra of condensed phase materials contain contributions that emerge, most intensely, from the surface and, with decreasing intensity, from various depths within the material (Fig. 3(a)). Previous steady-state studies have demonstrated

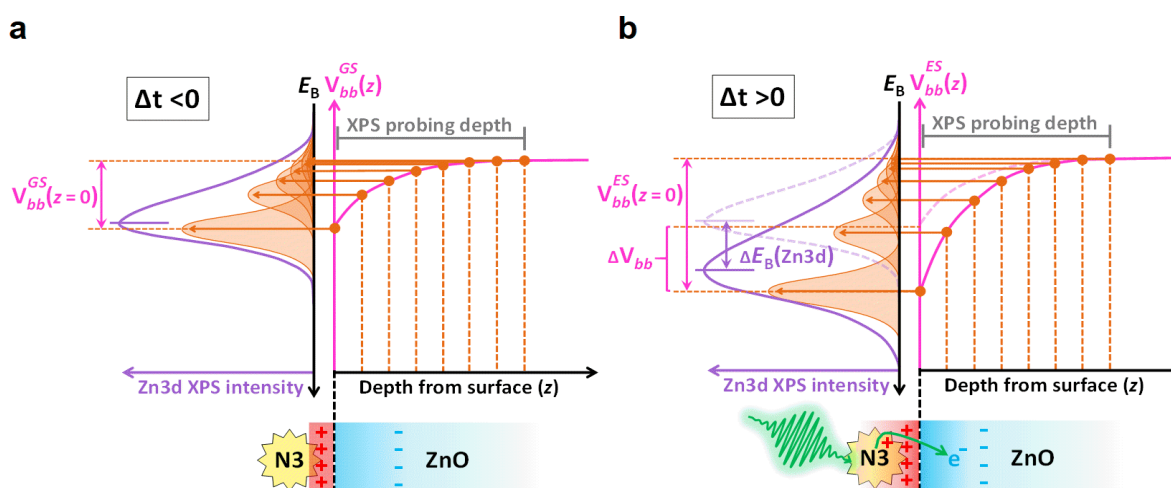


**Figure 3.** Schematic illustration of band bending effects in the Zn3d lineshape. The near-surface potential  $V_{bb}(z)$  (pink) within the ZnO space-charge region determines the binding energies of contributions from various depths (orange) to the overall Zn3d XPS signal for both, the ground state (a) and the photoexcited N3/ZnO junction (b). Light-induced charge injection enhances the pre-existing internal field and induces further downward band bending  $\Delta V_{bb}$ , which is larger than the apparent Zn3d peak shift  $\Delta E_B(\text{Zn3d})$  due to the averaging over different photoemission signals within the XPS probing depth. The correlation between XPS peak shifts and broadening encodes the spatial profile of  $V_{bb}(z)$ , which is retrieved by comparison of the Zn3d photoemission feature to numerical simulations (Fig. 4).

that the decomposition of XPS signal contributions from different depths can be used to reconstruct interfacial potential energy surfaces.<sup>32–35</sup> As described in the following, we translate this approach into the time domain to monitor the temporal evolution of the near-surface potentials in the ZnO substrate as a result of the photoexcitation of the interface (Fig. 3(b)). The technique is based on modeling the space-charge-induced fields and corresponding electronic structure of the hybrid junction in both the ground and excited states.

The GS band structure of the nanostructured ZnO substrate has been characterized by steady-state ultraviolet photoemission spectroscopy (UPS) and XPS,<sup>32</sup> and agrees with previously observed downward band-bending for bare and hydroxylated ZnO single-crystals under comparable vacuum conditions.<sup>36,37</sup> Subsequent N<sub>3</sub> adsorption has no significant impact on the semiconductor band structure (see SI section C). Therefore, the N<sub>3</sub>/ZnO heterojunction is characterized by the same surface potential as the bare ZnO substrate, which is schematically illustrated in Fig. 3(a). The GS band bending  $V_{bb}^{GS}(z)$  has a maximum at the surface  $V_{bb,max}^{GS} = V_{bb}^{GS}(z=0) = 0.79 \pm 0.03$  eV and is approximated by a cubic depth profile according to  $V_{bb}^{GS}(z) = V_{bb,max}^{GS} \cdot \left(\frac{z_{bb}^{GS}-z}{z_{bb}^{GS}}\right)^3$ , as reported in detail in ref. 32. Here,  $z_{bb}^{GS} = 5.1 \pm 0.7$  nm indicates the distance from the surface ( $z=0$ ) at which the electronic bands reach their bulk value. Note that this depth is the asymptotic limit of the band bending region, while the 1/e equivalent decay depth of the potential is  $z_{bb}^{dec} \approx 1.5$  nm. This band structure effectively represents a potential well for photo-injected electrons. We note that the significant band bending determined here and in ref. 32 is not necessarily expected for nanostructured semiconductors,<sup>38</sup> and makes surface properties (rather than those of the bulk) highly relevant for electron transport and photocatalytic

activity of nanoporous ZnO.<sup>29</sup> The pronounced band bending  $V_{bb}(z)$  inside the ZnO electrode has significant impact on the measured Zn3d lineshape, as the escape depth of the Zn3d photoelectrons in the soft X-ray region is comparable to  $z_{bb}^{dec}$ . The downward band bending results in a depth-dependent binding energy at different distances from the interface. This effect induces notable spectral broadening of the Zn3d lineshape and, conversely, opens up the possibility to reconstruct near-surface potential energy changes from an analysis of the Zn3d lineshape and peak shift. The depth-dependent surface potential analysis also provides access to the corresponding spatial distribution of the photo-injected carrier density  $\Delta n_e(z)$  via the Poisson relationship  $\frac{d^2 V_{bb}(z)}{dz^2} \propto n_e(z)$ , where  $n_e(z)$  is the electron density in the ZnO near-surface region. The validity of the model illustrated in Fig. 3 to assess transient electron density distributions in the substrate CB is confirmed by performing experiments at two significantly different photon energies, leading to different line broadenings and shifts, but the same physical conclusion, as outlined in the following. The shape of the potential has been extensively tested against possible alternatives, as described in ref. 32, clearly identifying the cubic depth-dependence as the most likely scenario.

As illustrated in Fig. 3(b), interfacial charge redistribution initiated by electron injection from the excited N3 dye into the semiconductor amplifies the pre-existing internal electric field, leading to an increased downward band bending of the electronic levels and, therefore, a shift to higher binding energies and further broadening of the Zn3d envelope. These correlated effects are used to quantify the photo-induced band bending dynamics at the molecule-semiconductor interface. A detailed description of this analysis is provided in section F of the SI. A key

benchmark that connects the measured trXPS spectra with the functional form of  $V_{bb}^{ES}(z)$  is the relation between the spectral shifts,  $\Delta E_B$ , and the spectral broadening,  $\Delta FWHM$ , as illustrated in Fig. 4. Shown are the observed excited state  $\Delta E_B(\text{Zn}3d)$  vs  $\Delta FWHM$  relations at X-ray photon energies of  $h\nu = 614$  eV (red diamonds) and  $h\nu = 320$  eV (blue squares), along with the results of

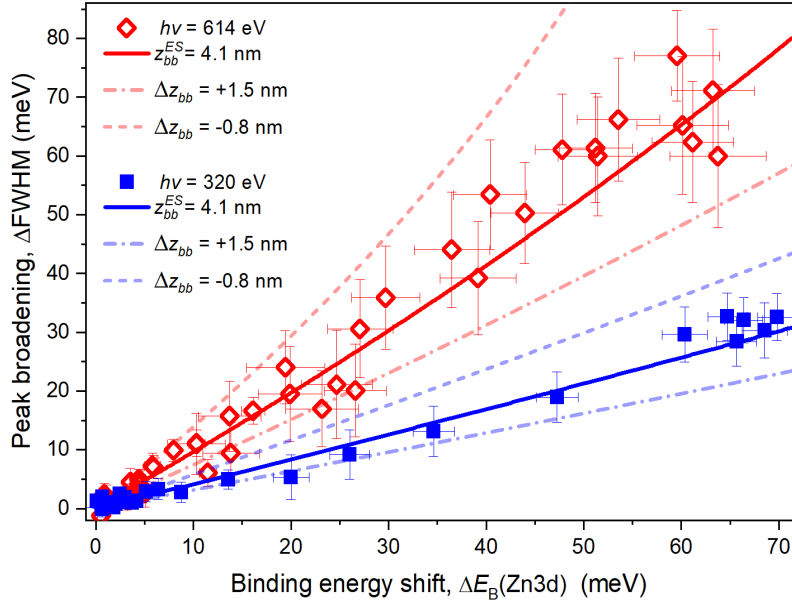


**Figure 4.** Evidence for nanoscale confinement of injected electrons at the interface. The correlation between the light-induced Zn3d XPS peak shifts and broadening measured with  $h\nu = 614$  eV (red diamonds) and  $h\nu = 320$  eV (blue squares) is compared to numerical simulations with a cubic band shape approximation for  $V_{bb}^{ES}(z)$ . A global parameter optimization on both datasets (solid lines) reveals a maximum spatial extent of the potential gradient below the ZnO surface of  $z_{bb}^{ES} = 4.1_{-0.8}^{+1.5}$  nm, and a light-induced modulation of the surface potential of  $\Delta V_{bb} = 100 \pm 20$  meV. The high spatial sensitivity of the modeling is demonstrated by comparing the data with predicted correlation traces for  $z_{bb}^{ES}$  variations according to its indicated uncertainty margins (dashed and dashed-dotted lines). Since the light-induced changes of  $V_{bb}(z)$  are directly linked to the injected charge density via the Poisson relation, these limits for the potential depth also restrict the spatial distribution of the injected charge carriers  $\Delta n_e(z)$  to the same length scale at the N3/ZnO interface.

a simulation (solid lines). The weak optical excitation of the N3 dyes for our experimental conditions ( $\approx 6\%$ , SI section G), induces relatively small modifications of  $V_{bb}^{GS}(z)$ . We therefore assume the same functional form for the photo-excited state potential of the heterojunction as for the ground state, i.e.,  $V_{bb}^{ES}(z) = V_{bb,max}^{ES} \times \left(\frac{z_{bb}^{ES}-z}{z_{bb}^{ES}}\right)^3$ . Note that the cubic form of  $V_{bb}(z)$  corresponds to a linear depth dependence if the electron density  $n_e(z)$  via the Poisson relationship. Using this potential shape and a convolution of spectral contributions from different depths  $z$  as described in section F of the SI, a global parameter optimization results in the solid lines shown in Fig. 4. Best agreement between the simulation and the two measurements is achieved for  $V_{bb,max}^{ES} = 0.89 \pm 0.04$  eV and  $z_{bb}^{ES} = 4.1_{-0.8}^{+1.5}$  nm (error limits indicate the parameter range where the  $\chi^2$  value of the fit is less than twice its minimum). This means that the interfacial electron injection further enhances the downward bending of the electronic levels below the ZnO surface by  $\sim 100$  meV. Simulation results for the upper and lower bounds for  $z_{bb}^{ES}$  are indicated by dash-dotted and dashed lines, respectively, in Fig. 4, demonstrating the sensitivity of the  $\Delta E_B(\text{Zn3d}) - \Delta \text{FWHM}$  correlation to small changes in  $z_{bb}$ . The two different photon energies used to record the datasets in Fig. 4 translate into a  $\sim 40\%$  difference in XPS sampling depth<sup>39</sup> (SI section F). The combination of both data sets therefore provides a rigorous test for evaluating the spatial dependence of  $V_{bb}^{ES}(z)$ . As expected, the  $h\nu = 320$  eV data exhibit larger peak shifts and less spectral broadening due to the smaller probing depth at this lower photon (and therefore electron kinetic) energy.

Due to the Poisson relation between potential gradients and charge carrier densities, the injected charge carrier distribution  $\Delta n_e(z)$  must be spatially confined to  $z \leq z_{bb}^{ES}$ , i.e. to a

maximum depth of  $\sim 6$  nm below the dye-semiconductor interface. This upper limit for the electron's penetration depth accounts for the uncertainty in the determination of  $z_{bb}^{ES}$  based on a planar sample surface model, while an isolated single sphere model would yield an even smaller value.<sup>32</sup> The actual surface topography of the ZnO films likely lies in between these two limiting cases.

We now turn to the interpretation of the transient C1s peak shifts  $\Delta E_B(\text{C1s})$  associated with the molecular component of the hybrid junction. Electronic states in chemisorbed monolayers experience the full change of the surface potential  $\Delta V_{bb}$ .<sup>40</sup> Thus, the observed maximum C1s peak shift  $\Delta E_B(\text{C1s}) = 180$  meV (Fig. 2(a), delay  $\Delta t = 2$  ns) consists of two contributions, the surface potential change  $\Delta V_{bb} = V_{bb,max}^{ES} - V_{bb,max}^{GS} \approx 100$  meV and a residual shift  $\Delta E_{N3} = \Delta E_B(\text{C1s}) - \Delta V_{bb} \approx 80$  meV. We attribute  $\Delta E_{N3}$  to the molecular response, representing the interfacial potential drop (IPD) between the oxidized N3 dye molecules and the ZnO surface. Quantitative analysis of the IPD provides direct access to interfacial charge configurations on a (sub-)nm scale. The IPD of a layer of charged molecules adsorbed to a solid substrate is approximated by a modified parallel-plate capacitor model that takes into account the charge density and dielectric properties of the molecules, as well as the average distance of the molecular charges from the surface.<sup>41</sup> Conversely, the distance of the charges from the substrate can be estimated from a known charge density and IPD. As described in section G of the SI, this procedure results in an estimate for the hole distance from the ZnO surface of  $\sim 0.3 - 1.2$  nm. This estimate corresponds approximately to the position of the Ru center atom and NCS groups, where most of the amplitude of the HOMO is located,<sup>21</sup> relative to the surface. In the photo-oxidized state of the dye, the hole density distribution is expected to closely resemble the HOMO

density distribution.<sup>21</sup> Values for the total height of the dye with respect to the substrate surface lie between 1.0 and 1.3 nm for different anchoring geometries on TiO<sub>2</sub>,<sup>19,42</sup> which is compatible with the retrieved hole-surface distance based on IPDs.

The interpretation of  $\Delta E_{N3}$  as the result of charge transfer from the dye to the substrate is corroborated by a trXPS study of photoexcited N3 molecules adsorbed on a gold substrate (see SI section I). Here, direct electron injection into the metal substrate and efficient screening of the injected charges is expected, corresponding to an immediate spectroscopic response from the ionized dye. Indeed, the C1s/Ru3d photolines in the N3/Au system exhibit an instrument-limited response similar to  $\Delta E_{N3}(\Delta t)$  (see SI Fig. S10). The molecular response of the N3/ZnO system also appears within the instrument response function (IRF) of the experiment. The IRF-limited onset of the dye oxidation strongly favors the fast population of intermediate ICT configurations, rather than intramolecular relaxation within a two-state model, as the reason for the previously observed delayed generation of free charge carriers in the ZnO CB.<sup>9,10,23</sup>

Closer inspection of the early time dynamics reveals a delayed rise of the ZnO-related trXPS signals compared to  $\Delta E_{N3}$ , see inset in Fig. 2(a). In this context, it is important to note that the excited electrons have to reside *inside* the ZnO semiconductor to alter the space-charge balance and the resulting internal potential  $V_{bb}(z)$ .<sup>17,29,30,33,40,43,44</sup> The combination of the instantaneous dye oxidation described above and the delayed response of  $\Delta E_B(\text{Zn3d})$  therefore provides clear evidence for a transient retention of the excited charge carriers in ICT states, before their release into the CB, on an overall timescale of  $\lesssim 1$  ns. These findings align with previous observations of delayed charge separation due to the intermediate population of ICT configurations.<sup>9,10,12,21</sup> Within this framework,  $\Delta E_B(\text{Zn3d})$  and  $(\Delta E_B(\text{C1s}) - \Delta E_{N3})$  are solely governed by the time-

dependent electron population in the CB of ZnO,  $P_{CB}(t)$ , whereas  $\Delta E_{N3}$  is defined by the net hole population in the N3 monolayer. Since population of ICT states ( $P_{ICT}(t)$ ) from HOMO-LUMO excited states is much faster than both intramolecular relaxation and the instrument response,<sup>10,15,21,45</sup> the hole population on the N3 dye molecules can be approximated by  $P_H(t) \approx P_{CB}(t) + P_{ICT}(t)$ . Based on these dynamic electron populations (Fig. 5), fits to first-order coupled rate equations are used to determine the mean ICT state lifetime from the transient energy shifts at  $\Delta t < 3$  ns (SI section H). The extracted ICT decay constant of  $300 \pm 80$  ps is consistent with timescales reported previously for injection intermediates at the N3/ZnO interface.<sup>9,10,23,46</sup> We note that  $\Delta E_{N3}(t) = \Delta E_B(C1s)(t) - \Delta E_B(Zn3d)(t)$  (not shown) exhibits indications for an overshoot of several ten meV immediately after photoexcitation, which vanishes on the same timescale as the ICT lifetime. This effect is consistent with previous observations that ICT states in the N3/ZnO system may, in addition to charge separation, also decay via electron-hole recombination on the dye.<sup>10</sup> Unfortunately, however, the density of data points in this time delay region is not sufficient to provide a quantitative estimate for the ratio of ICT decay by electron-hole recombination and charge injection into the ZnO CB.

We emphasize that the sensitization time of the ZnO electrodes was restricted to 3 min in order to exclude any surface degradation by dissolution of Zn ions from the electrode and formation of N3-Zn<sup>2+</sup> aggregates.<sup>15</sup> The observation of ICT state signatures in our work therefore establishes intermediate steps in the charge injection process as an intrinsic property of the pristine N3/ZnO interface. A recent valence photoemission study places the ICT state's center  $\sim 0.2$  eV above the CB minimum at the surface with a spectral width of  $\sim 0.8$  eV.<sup>24</sup> Combined with the excited-state downward band bending of  $\sim 0.89 \pm 0.04$  eV deduced here, it follows that even initially injected

‘hot’ electrons are not able to overcome the potential barrier separating the surface and core regions of individual nanoparticles of the ZnO nanoporous network. This distinct near-surface potential landscape points toward an anisotropic carrier mobility, with strong confinement

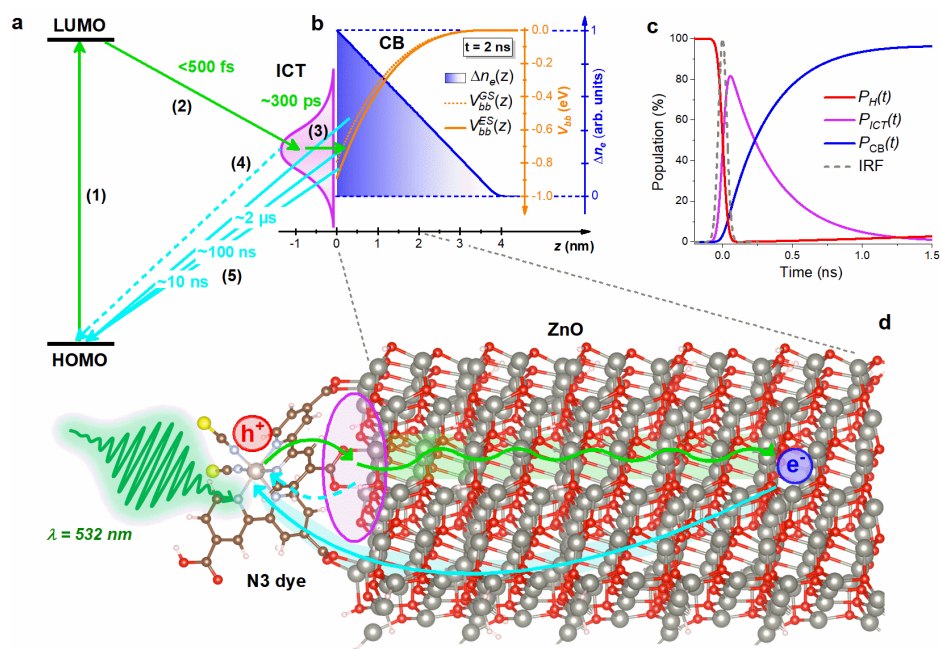


**Figure 5.** Spatio-temporal dynamics of the light-induced charge redistribution. **a** Schematic of the electron injection and recombination channels involved in the transient charge generation at the N3/ZnO hybrid interface. A lifetime of  $\sim 300$  ps for the ICT states is derived from a fit of the delayed onset of the Zn3d response shown in Fig. 2(a) to a coupled rate equation model for sequential 2-step injection. The long-term ( $\geq 10$  ns) relaxation timescales are determined by a fit of the ns- $\mu$ s dynamics in Fig. 2(a) to a tri-exponential decay. **b** Modulation of the CB minimum within the surface-near region of the ZnO nanoparticles (orange) and spatial distribution of the injected charge density  $\Delta n_e(z)$  at  $t = 2$  ns (blue, deduced from numerical modeling of the data as shown in Fig. 4). **c** Time-dependent population of HOMO electrons ( $P_H(t)$ ), ICT states ( $P_{ICT}(t)$ ) and the ZnO CB ( $P_{CB}(t)$ ) (IRF = instrument response function, populations are normalized to the number of excited electrons). **d** Illustration of the charge injection and recombination dynamics, using the energetically most favorable N3 adsorption geometry on a model ZnO(10 $\bar{1}$ 0) surface.

normal to the surface. Time-resolved THz and IR absorption studies<sup>9,12,23</sup> clearly indicate the existence of mobile charge carriers in the ZnO CB as a result of electron injection, but the results presented here show that these electrons do not penetrate into the nanoparticle bulk for particle sizes beyond ~15 nm. Thus, the most likely scenario for charge transport in such semiconductor substrates is lateral carrier diffusion along the interface.<sup>36</sup> This has general implications for ZnO-based photocatalytic devices, since near-interfacial diffusive transport of photo-excited carriers through nanoporous networks may activate additional surface-recombination pathways. These findings represent a possible explanation for the lower efficiencies of N3/ZnO devices compared to their TiO<sub>2</sub>-based counterparts. We note that additional measurements on N3/TiO<sub>2</sub> systems would be required for a more quantitative comparison. Generally, however, smaller band bending effects would be expected for TiO<sub>2</sub> nanoparticles due to the significantly higher dielectric constant of TiO<sub>2</sub> compared to ZnO.<sup>23,47</sup>

The long-term dynamics of the Zn3d and C1s energy shifts in Fig. 2(a) are well approximated by the sum of three exponentially decaying contributions (see SI section H), with relaxation times (relative amplitudes) of  $10 \pm 5$  ns (40%),  $100 \pm 30$  ns (30%) and  $2.0 \pm 0.3$   $\mu$ s (30%). These few-ns to few- $\mu$ s timescales fall within the range of recombination times previously observed for N3/ZnO junctions.<sup>14</sup> The appearance of three distinct recombination timescales, rather than a single stretched exponential decay, may point to the existence of distinct recombination pathways rather than a continuous distribution.<sup>48</sup> Further studies on ZnO electrodes with different types of impurities and well-controlled concentrations are necessary to reliably link individual decay times to specific recombination pathways, which is beyond the scope of this study.

The sequence of microscopic processes and their associated length scales that enable charge generation at the photo-excited N3/ZnO hybrid junction is schematically summarized in Fig. 5: (a) ultrafast HOMO-LUMO excitation of the dye (1) is followed by rapid (<500 fs) electron transfer to the ICT state (2). The ICT states depopulate on an overall timescale of ~300 ps by either transport of electrons into the CB of the ZnO nanoparticles (3) - leading to a modulation of the electric field inside the space-charge region - or electron-hole recombination (4). The recombination of injected electrons with the N3 HOMO-hole (5) proceeds through several relaxation pathways involving multiple timescales.<sup>14</sup>

The results presented here demonstrate the capability of trXPS to gain nanoscale insight into transient charge carrier distributions at complex interfaces. Both the injected electron density distribution (Fig. 5(b)) and the appearance and location of the HOMO hole remaining on the sensitizer are simultaneously characterized through the near-surface potential  $V_{bb}(z)$  and the interfacial potential drop, respectively. Note that, principally, trap states and their spatial distribution within the sample could have an impact on the reconstructed electron densities. However, as discussed in sections C and D of the SI, no direct evidence for trap states has been detected in either the bare or the sensitized sample. The fact that the same cubic potential depth profile, corresponding to a linearly varying electron density distribution, successfully describes the trXPS results for two different photon energies with two significantly different probing depths (Fig. 4), further indicates that trap states, if present, are unlikely to lead to significant deviations from the distributions outlined in Fig. 5(b).

The delay between the appearance of the HOMO hole and the modifications of  $V_{bb}(z)$  provides strong evidence for the intermediate population of ICT configurations (Fig. 5(b),(c)), as

the root cause for delayed charge injection. Quantitative insight into  $V_{bb}(z)$  reveals that the photo-injected electrons themselves enhance the already strong confinement along the surface normal within a  $<6$  nm wide region by increasing the  $\approx 0.79$  eV potential well depth of the ground state by an additional  $\approx 100$  meV. This finding is crucial for ZnO-based device designs, as the surface region of nanostructured ZnO electrodes seems to play a key role in facilitating charge transport. We note that the introduction of electrolyte environments in working devices may have some impact on the interfacial dynamics. However, as outlined in ref. 32, the pronounced band bending in the ground state ZnO substrate is the result of electron transfer doping from surface hydroxyl groups, formed upon contact of background water molecules with the ZnO surface. The study also strongly suggests that under the conditions of the trXPS experiment, the surface is fully hydroxylated. Thus, it is not clear how pronounced the impact of additional electrolyte molecules in the vicinity of the interface would be, but it would likely depend on their chemical nature. Future *in-operando* studies of complex hybrid systems, especially in the presence of electrolytes and with externally biased electrodes, feasible via ambient pressure trXPS, hold great potential to give a more complete picture of the spatio-temporal dynamics of carrier transport across these technologically pertinent interfaces under realistic working conditions.<sup>33,34</sup>

### *Experimental Methods*

The trXPS experiments were performed at Beamline 11.0.2 of the Advanced Light Source (ALS), using the HPPES (High Pressure Photoemission Spectroscopy) endstation<sup>49</sup> in

combination with a previously described time-tagging approach to enable picosecond time-resolved measurements.<sup>44,50,51</sup> The ALS was operated in two-bunch mode with an X-ray pulse spacing of 328.2 ns and an X-ray pulse duration of  $\sim 70$  ps. The 532 nm output of the pump laser system provided 10 ps long pulses at a repetition rate of 126.9 kHz and was synchronized to the ALS X-ray pulse train.<sup>50,51</sup> The X-ray beam was focused to a spot size of  $A_x = 70 \times 65 \mu\text{m}^2$ , whereas the laser spot size was adjusted to  $A_L = 165 \times 210 \mu\text{m}^2$ . Spatial overlap was achieved and maintained with an accuracy of  $<10 \mu\text{m}$ . The pump wavelength of 532 nm matches the absorbance maximum of the N3 dye in the visible regime (see SI Fig. S1(c)) and the employed pulse fluence of  $F_p = 1.1 \text{ mJ/cm}^2$  corresponds to an excitation probability of  $\approx 6\%$  (see section G of the SI for details).

### *Sample Characterization*

Details of the nanocrystalline ZnO electrode preparation, the characterization via scanning electron microscopy (SEM), as well as the sensitization process can be found in section A of the SI.

### *Statistical Analysis*

Details of the composition of the C1s/Ru3d XPS spectrum as well as the fit procedures to extract energy shifts and lineshape broadening effects from C1s/Ru3d and Zn3d spectra can be found in section B of the SI. An in-depth description of the procedure to retrieve ZnO near-surface potential gradients by numerical simulation of the Zn3d XPS spectra is given in section F of the SI.

## AUTHOR INFORMATION

### **Corresponding author**

Oliver Gessner, [ogessner@lbl.gov](mailto:ogessner@lbl.gov)

## Notes

The authors declare no competing financial interests.

## ACKNOWLEDGMENTS

This work was supported by the Atomic, Molecular, and Optical Sciences Program of the U.S. Department of Energy, Office of Science, Office of Basic Energy Sciences, Chemical Sciences, Geosciences and Biosciences Division, through Contract No. DE-AC02-05CH11231. The research used resources of the Advanced Light Source, which is a DOE Office of Science User Facility under contract no. DE-AC02-05CH11231. J.M. acknowledges support through the ALS Doctoral Fellowship in Residence Program. S.N. acknowledges financial support from the Alexander von Humboldt Foundation and the Helmholtz Association, and P.F. from the Deutsche Forschungsgemeinschaft (e-conversion Cluster of Excellence). F.R. acknowledges financial support by the VI 419 of the Helmholtz Association. FMT and GZ acknowledge support by the Liquid Sunlight Alliance, which is supported by the U.S. Department of Energy, Office of Science, Office of Basic Energy Sciences, Fuels from Sunlight Hub under Award Number DE-SC0021266. Support by Hendrik Bluhm during the experiments at ALS beamline 11.0.2 is greatly appreciated.

## SUPPORTING INFORMATION AVAILABLE:

A) Experimental details, sample preparation and characterization; B) Peak fitting analysis of the

trXPS spectra; C) Ground state electronic structure of the N<sub>3</sub>/ZnO interface; D) Control trXPS experiments on bare ZnO electrodes; E) Laser fluence dependence of trXPS effects; F) Retrieving potential gradients by numerical XPS peak simulations; G) Parallel plate capacitor model for interfacial potential drop; H) Rate equation model for 2-step charge injection and recombination; I) Time-resolved XPS of N<sub>3</sub> adsorbed to a gold substrate.

## REFERENCES

- (1) Hardin, B. E.; Snaith, H. J.; McGehee, M. D. The Renaissance of Dye-Sensitized Solar Cells. *Nat. Photonics* **2012**, *6*, 162–169.
- (2) Atwater, H. A.; Polman, A. Plasmonics for Improved Photovoltaic Devices. *Nat. Mater.* **2010**, *9*, 205–213.
- (3) Clavero, C. Plasmon-Induced Hot-Electron Generation at Nanoparticle/Metal-Oxide Interfaces for Photovoltaic and Photocatalytic Devices. *Nat. Photonics* **2014**, *8*, 95–103.
- (4) Grätzel, M. Solar Energy Conversion by Dye-Sensitized Photovoltaic Cells. *Inorg. Chem.* **2005**, *44*, 6841–6851.
- (5) Mubeen, S.; Lee, J.; Singh, N.; Krämer, S.; Stucky, G. D.; Moskovits, M. An Autonomous Photosynthetic Device in Which All Charge Carriers Derive from Surface Plasmons. *Nat. Nanotechnol.* **2013**, *8*, 247–251.
- (6) Hodes, G. Perovskite-Based Solar Cells. *Science* **2013**, *342*, 317–318.
- (7) Godin, R.; Kafizas, A.; Durrant, J. R. Electron Transfer Dynamics in Fuel Producing Photosystems. *Curr. Opin. Electrochem.* **2017**, *2*, 136–143.
- (8) Houle, F. A. Reaction–Transport Coupling in a Nanostructured Porous Electrode. *J. Phys. Chem. C* **2019**, *123*, 14459–14467.
- (9) Furube, A.; Katoh, R.; Hara, K.; Murata, S.; Arakawa, H.; Tachiya, M. Ultrafast Stepwise Electron Injection from Photoexcited Ru-Complex into Nanocrystalline ZnO Film via Intermediates at the Surface. *J. Phys. Chem. B* **2003**, *107*, 4162–4166.
- (10) Němec, H.; Rochford, J.; Taratula, O.; Galoppini, E.; Kužel, P.; Polívka, T.; Yartsev, A.; Sundström, V. Influence of the Electron-Cation Interaction on Electron Mobility in Dye-Sensitized ZnO and TiO<sub>2</sub> Nanocrystals: A Study Using Ultrafast Terahertz Spectroscopy. *Phys. Rev. Lett.* **2010**, *104*, 197401.
- (11) Stockwell, D.; Yang, Y.; Huang, J.; Anfuso, C.; Huang, Z.; Lian, T. Comparison of Electron-Transfer Dynamics from Coumarin 343 to TiO<sub>2</sub>, SnO<sub>2</sub>, and ZnO Nanocrystalline Thin Films: Role of Interface-Bound Charge-Separated Pairs. *J. Phys. Chem. C* **2010**, *114*, 6560–6566.

- (12) Strothkämper, C.; Bartelt, A.; Sippel, P.; Hannappel, T.; Schütz, R.; Eichberger, R. Delayed Electron Transfer through Interface States in Hybrid ZnO/Organic-Dye Nanostructures. *J. Phys. Chem. C* **2013**, *117*, 17901–17908.
- (13) Brauer, J. C.; Marchioro, A.; Paraecattil, A. A.; Oskouei, A. A.; Moser, J.-E. Dynamics of Interfacial Charge Transfer States and Carriers Separation in Dye-Sensitized Solar Cells: A Time-Resolved Terahertz Spectroscopy Study. *J. Phys. Chem. C* **2015**, *119*, 26266–26274.
- (14) Bauer, C.; Boschloo, G.; Mukhtar, E.; Hagfeldt, A. Electron Injection and Recombination in Ru(Dcbpy)<sub>2</sub>(NCS)<sub>2</sub> Sensitized Nanostructured ZnO. *J. Phys. Chem. B* **2001**, *105*, 5585–5588.
- (15) Horiuchi, H.; Katoh, R.; Hara, K.; Yanagida, M.; Murata, S.; Arakawa, H.; Tachiya, M. Electron Injection Efficiency from Excited N3 into Nanocrystalline ZnO Films: Effect of (N3–Zn<sup>2+</sup>) Aggregate Formation. *J. Phys. Chem. B* **2003**, *107*, 2570–2574.
- (16) Asbury, J. B.; Wang, Y.; Lian, T. Multiple-Exponential Electron Injection in Ru(Dcbpy)<sub>2</sub>(SCN)<sub>2</sub> Sensitized ZnO Nanocrystalline Thin Films. *J. Phys. Chem. B* **1999**, *103*, 6643–6647.
- (17) Zhang, Z.; Yates, J. T. Band Bending in Semiconductors: Chemical and Physical Consequences at Surfaces and Interfaces. *Chem. Rev.* **2012**, *112*, 5520–5551.
- (18) Ong, C. B.; Ng, L. Y.; Mohammad, A. W. A Review of ZnO Nanoparticles as Solar Photocatalysts: Synthesis, Mechanisms and Applications. *Renew. Sustain. Energy Rev.* **2018**, *81*, 536–551.
- (19) Chen, H.; Cole, J. M.; Stenning, G. B. G.; Yanguas-Gil, A.; Elam, J. W.; Stan, L.; Gong, Y. Imaging Dye Aggregation in MK-2, N3, N749, and SQ-2 Dye···TiO<sub>2</sub> Interfaces That Represent Dye-Sensitized Solar Cell Working Electrodes. *ACS Appl. Energy Mater.* **2020**, *3*, 3230–3241.
- (20) Mukaddem, K. T.; Chater, P. A.; Devereux, L. R.; Al Bahri, O. K.; Jain, A.; Cole, J. M. Dye-Anchoring Modes at the Dye···TiO<sub>2</sub> Interface of N3- and N749-Sensitized Solar Cells Revealed by Glancing-Angle Pair Distribution Function Analysis. *J. Phys. Chem. C* **2020**, *124*, 11935–11945.
- (21) Siefermann, K. R.; Pemmaraju, C. D.; Neppl, S.; Shavorskiy, A.; Cordones, A. A.; Vura-Weis, J.; Slaughter, D. S.; Sturm, F. P.; Weise, F.; Bluhm, H.; Strader, M. L.; Cho, H.; Lin, M.-F.; Bacellar, C.; Khurmi, C.; Guo, J.; Coslovich, G.; Robinson, J. S.; Kaindl, R. A.; Schoenlein, R. W.; Belkacem, A.; Neumark, D. M.; Leone, S. R.; Nordlund, D.; Ogasawara, H.; Krupin, O.; Turner, J. J.; Schlotter, W. F.; Holmes, M. R.; Messerschmidt, M.; Minitti, M. P.; Gul, S.; Zhang, J. Z.; Huse, N.; Prendergast, D.; Gessner, O. Atomic-Scale Perspective of Ultrafast Charge Transfer at a Dye–Semiconductor Interface. *J. Phys. Chem. Lett.* **2014**, *5*, 2753–2759.
- (22) Katoh, R.; Furube, A.; Yoshihara, T.; Hara, K.; Fujihashi, G.; Takano, S.; Murata, S.; Arakawa, H.; Tachiya, M. Efficiencies of Electron Injection from Excited N3 Dye into Nanocrystalline Semiconductor (ZrO<sub>2</sub>, TiO<sub>2</sub>, ZnO, Nb<sub>2</sub>O<sub>5</sub>, SnO<sub>2</sub>, In<sub>2</sub>O<sub>3</sub>) Films. *J. Phys. Chem. B* **2004**, *108*, 4818–4822.
- (23) Tiwana, P.; Docampo, P.; Johnston, M. B.; Snaith, H. J.; Herz, L. M. Electron Mobility and Injection Dynamics in Mesoporous ZnO, SnO<sub>2</sub>, and TiO<sub>2</sub> Films Used in Dye-Sensitized Solar Cells. *ACS Nano* **2011**, *5*, 5158–5166.

- (24) Borgwardt, M.; Wilke, M.; Kampen, T.; Mähl, S.; Xiao, M.; Spiccia, L.; Lange, K. M.; Kiyam, I. Yu.; Aziz, E. F. Charge Transfer Dynamics at Dye-Sensitized ZnO and TiO<sub>2</sub> Interfaces Studied by Ultrafast XUV Photoelectron Spectroscopy. *Sci. Rep.* **2016**, *6*, 24422.
- (25) Anderson, N. A.; Lian, T. ULTRAFAST ELECTRON TRANSFER AT THE MOLECULE-SEMICONDUCTOR NANOPARTICLE INTERFACE. *Annu. Rev. Phys. Chem.* **2005**, *56*, 491–519.
- (26) Benkö, G.; Kallioinen, J.; Myllyperkiö, P.; Trif, F.; Korppi-Tommola, J. E. I.; Yartsev, A. P.; Sundström, V. Interligand Electron Transfer Determines Triplet Excited State Electron Injection in RuN3–Sensitized TiO<sub>2</sub> Films. *J. Phys. Chem. B* **2004**, *108*, 2862–2867.
- (27) Kallioinen, J.; Benkö, G.; Sundström, V.; Korppi-Tommola, J. E. I.; Yartsev, A. P. Electron Transfer from the Singlet and Triplet Excited States of Ru(Dcbpy)<sub>2</sub>(NCS)<sub>2</sub> into Nanocrystalline TiO<sub>2</sub> Thin Films. *J. Phys. Chem. B* **2002**, *106*, 4396–4404.
- (28) Mayor, L. C.; Saywell, A.; Magnano, G.; Satterley, C. J.; Schnadt, J.; O’Shea, J. N. Adsorption of a Ru(II) Dye Complex on the Au(111) Surface: Photoemission and Scanning Tunneling Microscopy. *J. Chem. Phys.* **2009**, *130*, 164704.
- (29) Ozawa, K.; Emori, M.; Yamamoto, S.; Yukawa, R.; Yamamoto, S.; Hobara, R.; Fujikawa, K.; Sakama, H.; Matsuda, I. Electron–Hole Recombination Time at TiO<sub>2</sub> Single-Crystal Surfaces: Influence of Surface Band Bending. *J. Phys. Chem. Lett.* **2014**, *5*, 1953–1957.
- (30) Yukawa, R.; Yamamoto, S.; Ozawa, K.; Emori, M.; Ogawa, M.; Yamamoto, Sh.; Fujikawa, K.; Hobara, R.; Kitagawa, S.; Daimon, H.; Sakama, H.; Matsuda, I. Electron-Hole Recombination on ZnO(0001) Single-Crystal Surface Studied by Time-Resolved Soft X-Ray Photoelectron Spectroscopy. *Appl. Phys. Lett.* **2014**, *105*, 151602.
- (31) Gierster, L.; Vempati, S.; Stähler, J. Ultrafast Generation and Decay of a Surface Metal. *Nat. Commun.* **2021**, *12*, 978.
- (32) Mahl, J.; Gessner, O.; Barth, J. V.; Feulner, P.; Neppel, S. Strong Potential Gradients and Electron Confinement in ZnO Nanoparticle Films: Implications for Charge-Carrier Transport and Photocatalysis. *ACS Appl. Nano Mater.* **2021**, *4*, 12213–12221.
- (33) Favaro, M.; Jeong, B.; Ross, P. N.; Yano, J.; Hussain, Z.; Liu, Z.; Crumlin, E. J. Unravelling the Electrochemical Double Layer by Direct Probing of the Solid/Liquid Interface. *Nat. Commun.* **2016**, *7*, 1–8.
- (34) Lichterman, M. F.; Hu, S.; Richter, M. H.; Crumlin, E. J.; Axnanda, S.; Favaro, M.; Drisdell, W.; Hussain, Z.; Mayer, T.; Brunshwig, B. S.; Lewis, N. S.; Liu, Z.; Lewerenz, H.-J. Direct Observation of the Energetics at a Semiconductor/Liquid Junction by Operando X-Ray Photoelectron Spectroscopy. *Energy Environ. Sci.* **2015**, *8*, 2409–2416.
- (35) Shavorskiy, A.; Ye, X.; Karslıoğlu, O.; Poletayev, A. D.; Hartl, M.; Zegkinoglou, I.; Trotochaud, L.; Nemšák, S.; Schneider, C. M.; Crumlin, E. J.; Axnanda, S.; Liu, Z.; Ross, P. N.; Chueh, W.; Bluhm, H. Direct Mapping of Band Positions in Doped and Undoped Hematite during Photoelectrochemical Water Splitting. *J. Phys. Chem. Lett.* **2017**, *8*, 5579–5586.
- (36) Ozawa, K.; Mase, K. Metallization of ZnO(10-10) by Adsorption of Hydrogen, Methanol, and Water: Angle-Resolved Photoelectron Spectroscopy. *Phys. Rev. B* **2010**, *81*, 205322.

- (37) Ozawa, K.; Mase, K. Comparison of the Surface Electronic Structures of H-Adsorbed ZnO Surfaces: An Angle-Resolved Photoelectron Spectroscopy Study. *Phys. Rev. B* **2011**, *83*, 125406.
- (38) Hagfeldt, Anders.; Graetzel, Michael. Light-Induced Redox Reactions in Nanocrystalline Systems. *Chem. Rev.* **1995**, *95*, 49–68.
- (39) Tanuma, S.; Powell, C. J.; Penn, D. R. Calculation of electron inelastic mean free paths (IMFPs) VII. Reliability of the TPP-2M IMFP predictive equation. *Surf. Interface Anal.* **2003**, *35*, 268–275.
- (40) Gleason-Rohrer, D. C.; Brunschwig, B. S.; Lewis, N. S. Measurement of the Band Bending and Surface Dipole at Chemically Functionalized Si(111)/Vacuum Interfaces. *J. Phys. Chem. C* **2013**, *117*, 18031–18042.
- (41) Lueth, H. *Solid Surfaces, Interfaces and Thin Films*; 5th ed.; pp. 527-528; Springer: Berlin Heidelberg, 2010.
- (42) Cole, J. M.; Gong, Y.; McCree-Grey, J.; Evans, P. J.; Holt, S. A. Modulation of N3 and N719 Dye···TiO<sub>2</sub> Interfacial Structures in Dye-Sensitized Solar Cells As Influenced by Dye Counter Ions, Dye Deprotonation Levels, and Sensitizing Solvent. *ACS Appl. Energy Mater.* **2018**, *1*, 2821–2831.
- (43) Ozawa, K.; Yamamoto, S.; Yukawa, R.; Akikubo, K.; Emori, M.; Sakama, H.; Matsuda, I. Capturing Transiently Charged States at the C<sub>60</sub>/TiO<sub>2</sub>(110) Interface by Time-Resolved Soft X-Ray Photoelectron Spectroscopy. *Org. Electron.* **2016**, *31*, 98–103.
- (44) Neppl, S.; Gessner, O. Time-Resolved X-Ray Photoelectron Spectroscopy Techniques for the Study of Interfacial Charge Dynamics. *J. Electron Spectrosc. Relat. Phenom.* **2015**, *200*, 64–77.
- (45) Yoshihara, T.; Katoh, R.; Furube, A.; Murai, M.; Tamaki, Y.; Hara, K.; Murata, S.; Arakawa, H.; Tachiya, M. Quantitative Estimation of the Efficiency of Electron Injection from Excited Sensitizer Dye into Nanocrystalline ZnO Film. *J. Phys. Chem. B* **2004**, *108*, 2643–2647.
- (46) Anderson, N. A.; Ai, X.; Lian, T. Electron Injection Dynamics from Ru Polypyridyl Complexes to ZnO Nanocrystalline Thin Films. *J. Phys. Chem. B* **2003**, *107*, 14414–14421.
- (47) Goossens, A. Potential Distribution in Semiconductor Particles. *J. Electrochem. Soc.* **1996**, *143*, L131.
- (48) Phillips, J. C. Stretched Exponential Relaxation in Molecular and Electronic Glasses. *Rep. Prog. Phys.* **1996**, *59*, 1133.
- (49) Bluhm, H.; Andersson, K.; Araki, T.; Benzerara, K.; Brown, G. E.; Dynes, J. J.; Ghosal, S.; Gilles, M. K.; Hansen, H.-Ch.; Hemminger, J. C.; Hitchcock, A. P.; Ketteler, G.; Kilcoyne, A. L. D.; Kneedler, E.; Lawrence, J. R.; Leppard, G. G.; Majzlam, J.; Mun, B. S.; Myneni, S. C. B.; Nilsson, A.; Ogasawara, H.; Ogletree, D. F.; Pecher, K.; Salmeron, M.; Shuh, D. K.; Tonner, B.; Tyliszczak, T.; Warwick, T.; Yoon, T. H. Soft X-Ray Microscopy and Spectroscopy at the Molecular Environmental Science Beamline at the Advanced Light Source. *J. Electron Spectrosc. Relat. Phenom.* **2006**, *150*, 86–104.
- (50) Neppl, S.; Shavorskiy, A.; Zegkinoglou, I.; Fraund, M.; Slaughter, D. S.; Troy, T.; Ziemkiewicz, M. P.; Ahmed, M.; Gul, S.; Rude, B.; Zhang, J. Z.; Tremsin, A. S.; Glans, P.-A.; Liu, Y.-S.; Wu, C. H.; Guo, J.; Salmeron, M.; Bluhm, H.; Gessner, O. Capturing

Interfacial Photoelectrochemical Dynamics with Picosecond Time-Resolved X-Ray Photoelectron Spectroscopy. *Faraday Discuss.* **2014**, *171*, 219–241.

- (51) Shavorskiy, A.; Neppl, S.; Slaughter, D. S.; Cryan, J. P.; Siefermann, K. R.; Weise, F.; Lin, M.-F.; Bacellar, C.; Ziemkiewicz, M. P.; Zegkinoglou, I.; Fraund, M. W.; Khurmi, C.; Hertlein, M. P.; Wright, T. W.; Huse, N.; Schoenlein, R. W.; Tyliszczak, T.; Coslovich, G.; Robinson, J.; Kaindl, R. A.; Rude, B. S.; Ölsner, A.; Mähl, S.; Bluhm, H.; Gessner, O. Sub-Nanosecond Time-Resolved Ambient-Pressure X-Ray Photoelectron Spectroscopy Setup for Pulsed and Constant Wave X-Ray Light Sources. *Rev. Sci. Instrum.* **2014**, *85*, 093102.